Lasing with conical diffraction feature in the KGd(WO 4) 2 :Nd biaxial crystal

Alain Brenier

Appl. Phys. B (2016) 122:237
DOI 10.1007/s00340-016-6512-y

Lasing with conical diffraction feature in the $KGd(WO_4)_2$:Nd biaxial crystal

Alain Brenier
Univ Lyon, Université Claude Bernard Lyon 1, CNRS, Institut Lumière Matière, F-69622, LYON, France
alain.brenier@univ-lyon1.fr

Abstract : With an experimental set-up designed to record simultaneously the far field and the near field patterns, we got lasing with feature of conical diffraction in the biaxial Nd^{3+}-doped $KGd(WO_4)_2$ crystal. The key-point is that the lasing direction is not single and is constituted by an angular distribution including the optical axis. Very slight changes of crystal orientation leads to crescent shape 1068 nm light distributions in the near field. The beam launched towards the biaxial crystal is mainly linear polarized with its intensity in agreement with the Nd fluorescence angular distribution. A theoretical background is provided, including the monoclinic and triclinic symmetries and laser amplification including elliptical modes and cavity round trip.

Keywords: conical diffraction; biaxial crystal; optical axis; diode pumped laser

1. Introduction

Pleochroism in biaxial anisotropic crystals was recognized more than a century ago. This phenomenon is the result of the polarization dependence of the light absorption due to dopants or various color centers. For propagation directions close to the optical axes, the plane-wave modes (far field detection) which propagates unchanged are elliptically polarized [1-3] and we expect also this behaviour for stimulated emission. This latter case is studied in [4] for the Nd^{3+}-doped $KGd(WO_4)_2$ (KGW) biaxial laser crystal. The anisotropy of the absorption (or amplification) splits an optical axis in two new ones, each propagating unchanged a right or left circularly polarized light. Launching the inverse circular polarization, i. e. left or right respectively, leads to propagation of the singular Voigt wave [3-5]. Its existence in a medium depends on a key parameter [6]. This wave could find applications in optical sensing [7], for example from a porous biaxial dielectric.

On another hand in the near field, the wave propagation along an optical axis of a transparent biaxial crystal leads to internal conical refraction [8-9]: the focused flux of light energy is split into a cone and finally rings instead of being doubly-refracted as in the other wave directions. Several opticians studied experimentally this phenomenon (Poggendorf rings, Raman spot and so on) in the two last centuries and its theoretical description was obtained [10-14]. Nowadays a few applications have emerged: polarization demultiplexing and multiplexing [15] for free-space optical communication, optical trapping of micro-spheres [16], enhanced resolution microscopy by sub-wavelength localisation [17-18], two-photon polymerisation [19], and polarimetry [20-21]. The agreement between the theoretical description and experimental data has been extensively published recently in the far field [22-23] as well as imaging the near field [24-29].

Applications of optical axis-oriented biaxial doped crystals exist also in the field of lasers. A KGW:Yb^{3+} laser was built with a polarization state selected in an arbitrarily direction without any additional cavity component [30], simply by moving the pump area inside the gain medium. A high quality Gaussian beam was obtained [31-32] emerging from the output plane mirror after being generated along the optical axis of a KGW:Nd^{3+} crystal. In contrast, the light energy output was found distributed inside a crescent-shaped area in [33-34] which is more similar with the characteristic focused conical refraction pattern. So, the conical refraction/diffraction is clearly more complicated when it occurs inside a laser cavity. This is also what we have experienced in the present work as we show below, due to the fact that the experimenter does not control the generated beam going through the crystal: the latter results of complex interactions with the anisotropic stimulated emission gain and is in fact a property of the system itself. For this reason we could speak of "self-conical diffraction". In this context, the present study includes both far field and near field complementary behaviors, the far field revealing the optical axis position inside the laser angular distribution as well as the polarization distribution.

This work is organized as follow. Section 2 is devoted to a theoretical background including the case of monoclinic and triclinic symmetries and laser amplification including elliptical modes and cavity round trip (chirality is also included despite not necessary here). The experimental method in section 3 explains how different conical diffraction patterns can be obtained from very slightly different KGW:Nd^{3+} laser crystal orientations inside the cavity, all with a propagation direction distribution of lasing including the optical axis direction. Section 4 is devoted to results and modelling.

2. Theoretical background

2.1 Plane wave refraction

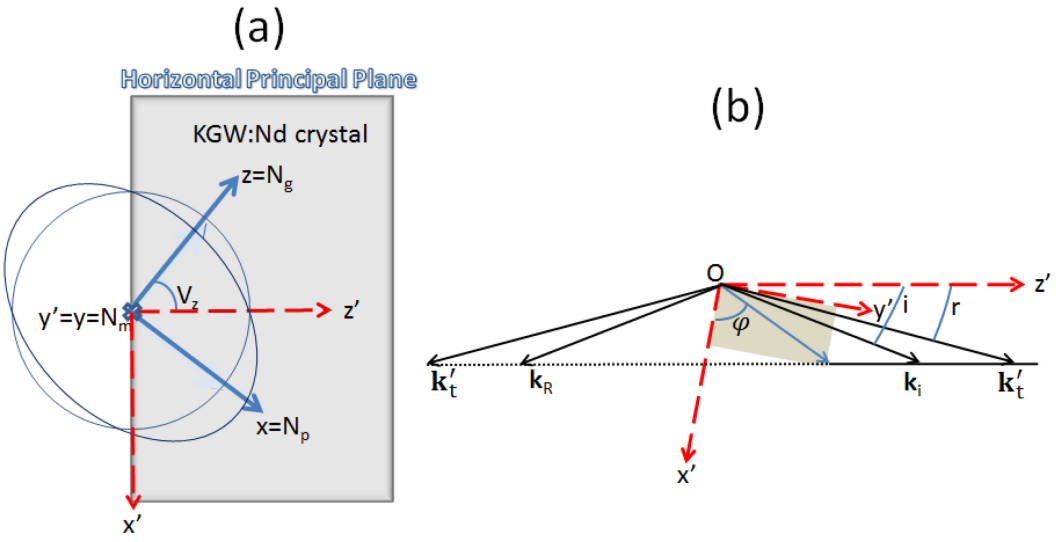

Fig. 1 (a) Crystal orientation and useful frameworks, (b) refraction law illustrated in the incidence plane (=Figure plane; the Ox'y' face is perpendicular to the incidence plane).

We use a first (x', y', z') cartesian framework linked to the crystal as it is shown in Fig. 1 (a). An incident plane wave ($\mathbf{k}_i$ wave-vector) launched on the x'Oy' entrance face of the crystal generates an inhomogeneous refracted (transmitted) wave with a $\mathbf{k}_t=\mathbf{k}'_t + i\,\mathbf{k}''_t$ wave-vector (Fig. 1 (b)). Another cartesian frame ($\mathbf{x_1}$, $\mathbf{x_2}$, $\mathbf{x_3}$) is needed: its third axis $\mathbf{x_3}$ is parallel to the real refracted wave-vector $\mathbf{k}'_t(r,\varphi)$ ($(r,\ \varphi)$: polar and azimuthal angles) so it is transverse and it coincides locally with the $\mathbf{e}_{\theta=r}$, $\mathbf{e}_{\phi}$, $\mathbf{e}_{k'}$ unit vectors of the spherical coordinates.

The refraction law is given by the equality of the tangential components of the wave-vectors with three results. First $\mathbf{k}'_t$ is in the incidence plane, secondly the refracted polar angle can be calculated from $\sin(r) = \sin(i)\,\mathrm{k}_i/\mathrm{k}'_t$ and third the k''_{t1} transverse component can be calculated from the k''_{t3} longitudinal one by: $\mathrm{k}''_{t1} = \mathrm{k}''_{t3}\, tg(r)$. Because the imaginary part is much smaller than the real one and because we will use only incidences close to the normal incidence ($\mathrm{k}''_{t1} \ll \mathrm{k}''_{t3}$), we can make two approximations. First we simplify the calculation of the refraction angle by using an average refractive index $\mathrm{n_{moy}}$ inside the crystal, so: $\mathrm{k}'_t = 2\pi n_{moy}/\lambda$ and secondly we will neglect the transverse component k''_{t1} and we will treat the refracted wave as homogeneous.
In summary, the *r* refraction and φ Euler angles which appear along the following calculation will be obtained from the $(k_{ix'}, k_{iy'})$ tangential components by:

$$\sin(r) = \frac{\left[k_{ix'}^2 + k_{iy'}^2\right]^{1/2}}{2\pi n_{moy}/\lambda} \quad (1)$$

$$\cos(\varphi) = \frac{k_{ix'}}{\left[k_{ix'}^2 + k_{iy'}^2\right]^{1/2}} \quad (2)$$

The last useful detail is to examine how are the wave-vector $\mathbf{k}_\mathrm{R}$ of the wave reflected back on a mirror orthogonal to z' axis (in the next section it will be the output cavity mirror) and the wave-vector $\mathbf{k}_\mathrm{Rt}$ of the wave reflected and then transmitted inside the crystal. Inspection of Fig. 1 (b) reveals that the polar angle of $\mathbf{k}_\mathrm{Rt}$ is $\pi - r$ while the φ azimuthal angle is unchanged.

2.2 Propagation of the refracted plane wave in the transverse framework ($\mathbf{x_1}$, $\mathbf{x_2}$, $\mathbf{x_3}$)
Let us exhibit several relations useful below. The electromagnetic wave properties such as the polarizations and spectroscopy (absorption and amplification coefficients in cm^{-1}) of a laser material are fully obtained in any direction of propagation for the two modes from the linear permittivity tensor:

$$\varepsilon = \varepsilon_0(\epsilon' + i\epsilon'') \quad (3)$$

through Maxwell equations. In the so-called $\mathrm{x=N_p}$, $\mathrm{y=N_m}$, $\mathrm{z=N_g}$ dielectric frame, where at this step we have written equation (3), the real part (related to the refraction indices: $\varepsilon'_{ii} = n_i^2$) is diagonal but the imaginary part is not in the monoclinic and triclinic crystal symmetries or in case of gyrotropy.
Due to the transverse nature of the dielectric displacement vector $\mathbf{D}$, it is convenient to work in the ($\mathbf{x_1}$, $\mathbf{x_2}$, $\mathbf{x_3}$) transverse frame. The following relation occurs between the three components of the electric field $\widehat{\boldsymbol{E}}$:

$$\hat{E}_3 = -\frac{\underline{\epsilon}_{31}\hat{E}_1 + \underline{\epsilon}_{32}\hat{E}_2}{\underline{\epsilon}_{33}} \quad (4)$$

More, the permittivity tensor is expressed as $\underline{\varepsilon}$:

$$\underline{\varepsilon}(r,\varphi) = S_2(r,\varphi)(S_1 \varepsilon S_1^{-1})S_2^{-1}(r,\varphi) \quad (5)$$

where $S_1$is the 3-D rotation making the (x, y, z)→(x', y', z') frame transfer and $S_2(r,\varphi)$ makes the (x', y', z')→($\mathrm{x_1}$, $\mathrm{x_2}$, $\mathrm{x_3}$) transfer (see Fig. 1 (b)). The relative position of the two (x,

y, z) and (x', y', z') frames can be any but in the peculiar case of the optical axis oriented crystal such as Fig. 1 (a) S_1 is simply:

$$S_1 = \begin{bmatrix} \cos(V_z) & 0 & -\sin(V_z) \\ 0 & 1 & 0 \\ sin(V_z) & 0 & cos(V_z) \end{bmatrix} \quad (6)$$

V_z being the angle between the optical axis and **z**, whereas:

$$S_2(r,\varphi) = \begin{bmatrix} \cos(r)\cos(\varphi) & \cos(r)\cos(\varphi) & -\sin(r) \\ -\sin(\varphi) & \cos(\varphi) & 0 \\ \sin(r)\cos(\varphi) & \sin(r)\sin(\varphi) & \cos(r) \end{bmatrix} \quad (7)$$

Let us use the notations [4, 6]:

$$\begin{aligned} \delta_{11} &= \underline{\epsilon}_{11}\underline{\epsilon}_{33} - \underline{\epsilon}_{13}\underline{\epsilon}_{31} \\ \delta_{12} &= \underline{\epsilon}_{12}\underline{\epsilon}_{33} - \underline{\epsilon}_{13}\underline{\epsilon}_{32} \\ \delta_{21} &= \underline{\epsilon}_{21}\underline{\epsilon}_{33} - \underline{\epsilon}_{23}\underline{\epsilon}_{31} \\ \delta_{22} &= \underline{\epsilon}_{22}\underline{\epsilon}_{33} - \underline{\epsilon}_{23}\underline{\epsilon}_{32} \end{aligned}$$

(8)

The propagation modes are found inserting $\mathbf{E}(x_3)\exp(ik\,x_3)$ solutions in the propagation equations and the result is the Fresnel equation which is the characteristic equation of the 2-dimension eigen-value problem. Its roots are the two wavenumbers given by the following formula:

$$k_+(r,\varphi) = \omega\left[\frac{\mu_0}{2\underline{\epsilon}_{33}}\left\{(\delta_{11}+\delta_{22}) + \Delta^{1/2}\right\}\right]^{1/2} \quad (9)$$

$$k_-(r,\varphi) = \omega\left[\frac{\mu_0}{2\underline{\epsilon}_{33}}\left\{(\delta_{11}+\delta_{22}) - \Delta^{1/2}\right\}\right]^{1/2} \quad (10)$$

with $\Delta = (\delta_{11}-\delta_{22})^2 + 4\delta_{12}\delta_{21}$ being the discriminant of the Fresnel equation.

The polarizations of the two eigen-modes are found to have the transverse components:

$$\left[\frac{1}{\frac{\delta_{22}-\delta_{11}\pm\Delta^{1/2}}{2\delta_{12}}}\right]_{x1x2} \quad (11)$$

in the ($\mathbf{x_1}$, $\mathbf{x_2}$, $\mathbf{x_3}$) frame in such a way that the transverse eigen-modes frame→ ($\mathbf{x_1}$, $\mathbf{x_2}$) transfer is operated by the matrix:

$$S_3 = \begin{bmatrix} 1 & 1 \\ \frac{\delta_{22}-\delta_{11}+\Delta^{1/2}}{2\delta_{12}} & \frac{\delta_{22}-\delta_{11}-\Delta^{1/2}}{2\delta_{12}} \end{bmatrix} \quad (12)$$

2.3 Far field pattern

The electric field $\boldsymbol{E}$ of the input beam at the entrance face of the crystal is a priori known in the (x', y', z') frame and can be decomposed in plane waves from its 2D-Fourier transform $\widehat{\boldsymbol{E}}$. So its two tangential components are: $\begin{bmatrix}\hat{E}_{x'}(k_{ix'},k_{iy'})\\ \hat{E}_{y'}(k_{ix'},k_{iy'})\end{bmatrix}$. The refraction is such that the tangential electric field is continuous on the air/crystal separation surface but in the present work we will use an anti-reflection coating so reflexion is neglected and the tangential electric field is transmitted. Then three steps are needed to calculate their spatial evolution through the crystal.

-step 1: we obtain the $\widehat{\boldsymbol{E}}$ tangential components in the ($\mathbf{x}_1$, $\mathbf{x}_2$) transverse frame:

$$\begin{bmatrix}\hat{E}_1(k_{ix'},k_{iy'})\\ \hat{E}_2(k_{ix'},k_{iy'})\end{bmatrix}=\begin{bmatrix}\cos(r)\cos(\varphi) & \cos(r)\cos(\varphi)\\ -\sin(\varphi) & \cos(\varphi)\end{bmatrix}\begin{bmatrix}\hat{E}_{x'}(k_{ix'},k_{iy'})\\ \hat{E}_{y'}(k_{ix'},k_{iy'})\end{bmatrix} \quad (13)$$

where the square matrix is $S_2(r,\varphi)$ restricted to its tangential part.

-step 2: with the help of the eigen-modes we obtain the $\widehat{\boldsymbol{E}}$ tangential components after *L=e/cos(r)* length path crossed inside the crystal (thickness: *e*):

$$\begin{bmatrix}\hat{E}_1(L,k_{ix'},k_{iy'})\\ \hat{E}_2(L,k_{ix'},k_{iy'})\end{bmatrix}=S_3\begin{bmatrix}e^{ik_+L} & 0\\ 0 & e^{ik_-L}\end{bmatrix}S_3^{-1}\begin{bmatrix}\hat{E}_1(k_{ix'},k_{iy'})\\ \hat{E}_2(k_{ix'},k_{iy'})\end{bmatrix} \quad (14)$$

and consequently dropping the $(k_{ix'},k_{iy'})$ notation: $\hat{E}_3(L)=-\frac{\underline{\epsilon}_{31}\hat{E}_1(L)+\underline{\epsilon}_{32}\hat{E}_2(L)}{\underline{\epsilon}_{33}}$

-step 3: we go back to the (x', y', z') frame with a compressed notation:

$$\left[\widehat{\boldsymbol{E}}(L,k_{ix'},k_{iy'})\right]_{x'y'z'}=S_2^{-1}(r,\varphi)\left[\widehat{\boldsymbol{E}}(L,k_{ix'},k_{iy'})\right]_{x1x2x3} \quad (15)$$

The two first components are the tangential ((x', y') frame) wanted far field from which we can obtain the wave intensity by the hermitian scalar product after eventually multiplication by the 2X2 Jones matrix representing any polarizer (linear or circular) located at the exit face of the crystal.

2.4 Near field pattern

Expression (15) gives the electric field 2D-Fourier transform at the exit face of the crystal. After propagation in air over a distance d, the Fourier transform is multiplied by $\exp(ik_{iz'}d)$ with $k_{iz'}=\left((\frac{2\pi}{\lambda})^2-(k_{ix'}^2+k_{iy'}^2)\right)^{1/2}$. All the plane waves interfere, in other words the electric field is obtained as the inverse 2D-Fourier transform *iFT* (transverse x'y' components in a compressed notation):

$$[\boldsymbol{E}(x',y',d)]_{x'y'}=iFT\left\{\exp(ik_{iz'}d)\left[\widehat{\boldsymbol{E}}\left(L,k_{ix'},k_{iy'}\right)\right]_{x'y'}\right\} \quad (16)$$

The intensity of the near field transmitted wave is obtained from the hermitian scalar product, whereas the phase wave front is obtained as the imaginary part of the field components.

2.5 The case of the KGW:Nd symmetry

The KGW:Nd crystal belongs to the C2/c space group, it is monoclinic and centrosymmetric. The two-fold **b** crystallographic axis coincides with the **Np**=**x** (=**b**) principal axis of the dielectric frame. The two other **Nm**=**y** and **Ng**=**z** principal axes lie in the **a-c** crystallographic plane with a known orientation [35], but this latter has no role in the present optical study.
To obtain the real part of the tensor (3) we chose to recalculate the and n_p and n_g refractive indices values (and keeping n_m=1.986 [35]) in order to get simultaneously the V_z=46.6° polar angle of the optical axis [36], and anticipating the study given in the next section 3, the first dark ring radius (0.3285°) from far field conoscopy at 1064 nm and the semi-angle A (0.96°) of the hollow cone from internal conical refraction. This procedure was used because refractive indices previous published values failed to yield the experimental data (this situation was similar in [5]). The result is n_p=1.9516and n_g=2.0183.
The imaginary part of Eq. (3) is symmetric because no chirality exists for centric structures and in addition it is diagonal in a $(\tilde{x}, \tilde{y}, \tilde{z})$ frame deduced by a θ_0 rotation of the x, y, z frame around the **x** (=**b**) axis as it is allowed by the monoclinic symmetry. This rotation means that generally absorption and fluorescence extrema do not coincide with the three principal x, y, z axes. A nondiagonal term ε''_{yz} appears if we express ε" in the xyz frame from its diagonal expression in the $(\tilde{x}, \tilde{y}, \tilde{z})$ frame:

$$\begin{bmatrix} \varepsilon''_{xx} & 0 & 0 \\ 0 & \varepsilon''_{yy} & \varepsilon''_{yz} \\ 0 & \varepsilon''_{yz} & \varepsilon''_{zz} \end{bmatrix} = \begin{bmatrix} 1 & 0 & 0 \\ 0 & \cos(\theta_0) & \sin(\theta_0) \\ 0 & -sin(\theta_0) & \cos(\theta_0) \end{bmatrix} \begin{bmatrix} \varepsilon''_{\tilde{x}\tilde{x}} & 0 & 0 \\ 0 & \varepsilon''_{\tilde{y}\tilde{y}} & 0 \\ 0 & 0 & \varepsilon''_{\tilde{z}\tilde{z}} \end{bmatrix} \begin{bmatrix} 1 & 0 & 0 \\ 0 & \cos(\theta_0) & -\sin(\theta_0) \\ 0 & \sin(\theta_0) & \cos(\theta_0) \end{bmatrix}$$

(17)

We have the relations: $k''_{\tilde{\imath}} = N\sigma_{\tilde{\imath}} = 2\pi/(n_{\tilde{\imath}}\lambda)\varepsilon''_{\tilde{\imath}\tilde{\imath}}$ where N is the population inversion for amplification and $\sigma_{\tilde{\imath}}$ the stimulated emission cross-section: σ_p=11.93 10^{-20} cm^2, σ_m=32.26 10^{-20} cm^2, σ_g=8.30 10^{-20} cm^2 [37].
Inspection of $\boldsymbol{\varepsilon}''_{ij}$ reveals that the θ_0 angle can be obtained from the formula:

$$tg(2\theta_0) = \frac{2\varepsilon''_{yz}}{\varepsilon''_{zz} - \varepsilon''_{yy}} \qquad (18)$$

Such a rotation (θ_0#10°) was reported for KGW:Nd [4] and it was already encountered in the monoclinic YCOB:Nd [38]. Its wavelength dependence imposes it as a fourth spectroscopic parameter for monoclinic crystals [39-40].

3. Experimental methods

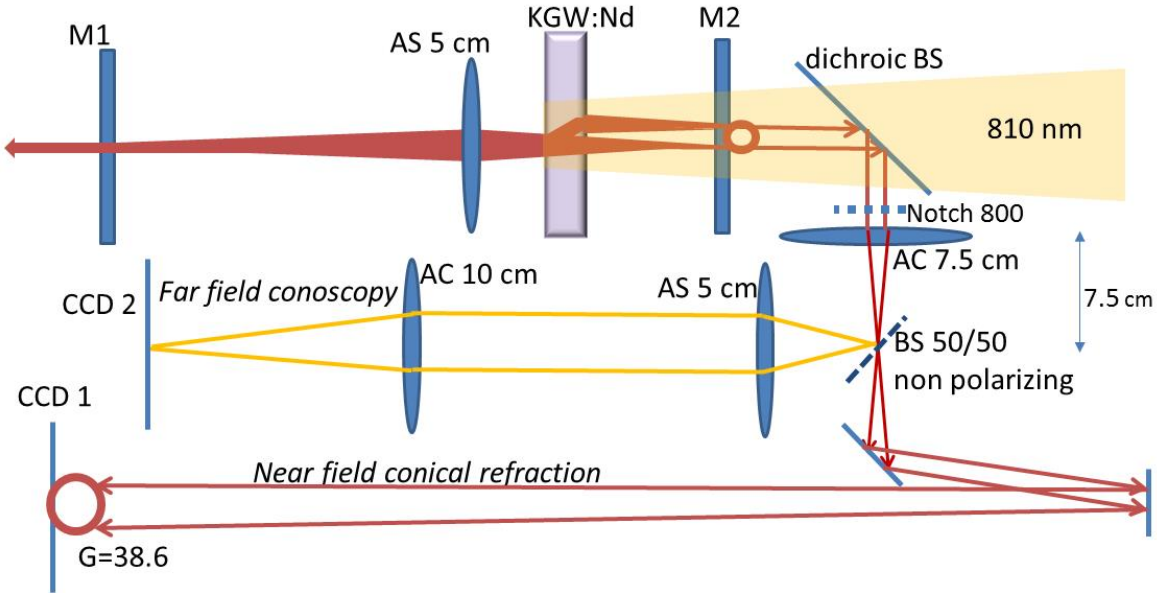

Fig. 2 Lasing set-up and optical paths for far field and near field analysis.

The crystal is pumped through a dichroic beamsplitter at 810 nm with a fibre coupled Limo laser diode (0.22 NA and 200 µm diameter). The KGW:Nd crystal has 3% Nd doping and has 3.15 mm thickness.

The laser cavity (Fig. 2) is defined par the two plane mirrors M1 (5% T@1068 nm) and M2 (2%T@1068 nm) and it is stabilized by an AR aspherical lens with 5 cm focal length. Various sizes of the two arms were tried (in the shorter one is located the KGW:Nd crystal), leading to various beam waists on the M2 mirror. The laser results presented in section 4 were obtained with 16.5 cm and 6.5 cm arm lengths, which led to about 55 µm beam waist on the M2 mirror. This value was judged satisfying since it is close to the conical refraction ring radius for a 3 mm thick KGW crystal (52 µm according to our measurement) and allows a doughnut-like near field pattern frequently observed in conical refraction experiments. Shortening the M1 arm up to 7 cm increased the laser waist up to 220 µm, suppressing any structure in the near field. The KGW-M2 distance was close to 1.7 cm. Various KGW-M2 mirror distances were also tried, up to 0.3 cm, but with similar results.

Lasing occured at 1068 nm. A polarizer and a power meter can be installed towards the M1 laser output. The M2 laser output is analysed along two optical paths: one for imaging (CCD 2) the far field which is present at the focal plane located at 7.5 cm of an achromatic lens (AC 7.5 cm), the second one for imaging on the CCD 1 the field intensity distribution (near field) located on the M2 mirror by the AC 7.5 cm lens correctly adjusted for a clear image with G=38.6 estimated magnification. On the far field conoscopy path, two achromatic AC 10 cm and AC 5 cm lenses are installed, first to have 2 time magnification of the far field size and second to accommodate a quarter wave plate (fast axis at 45°) and/or a linear polarizer (both to constitute a circular polarizer).

The KGW:Nd sample is inserted in a water cooled copper holder equipped for rotation around with three orthogonal axis (one longitudinal and two transverse). The longitudinal axis rotation was used to orient horizontally the N_p-N_g principal plane from 1064 nm far field conoscopy with a similar procedure than [4]. This orientation (see Fig. 1 (a)) was keeping fixe all along the experiment.

Lasing was studied after the thermal stabilization was reached.

4. Results and modelling

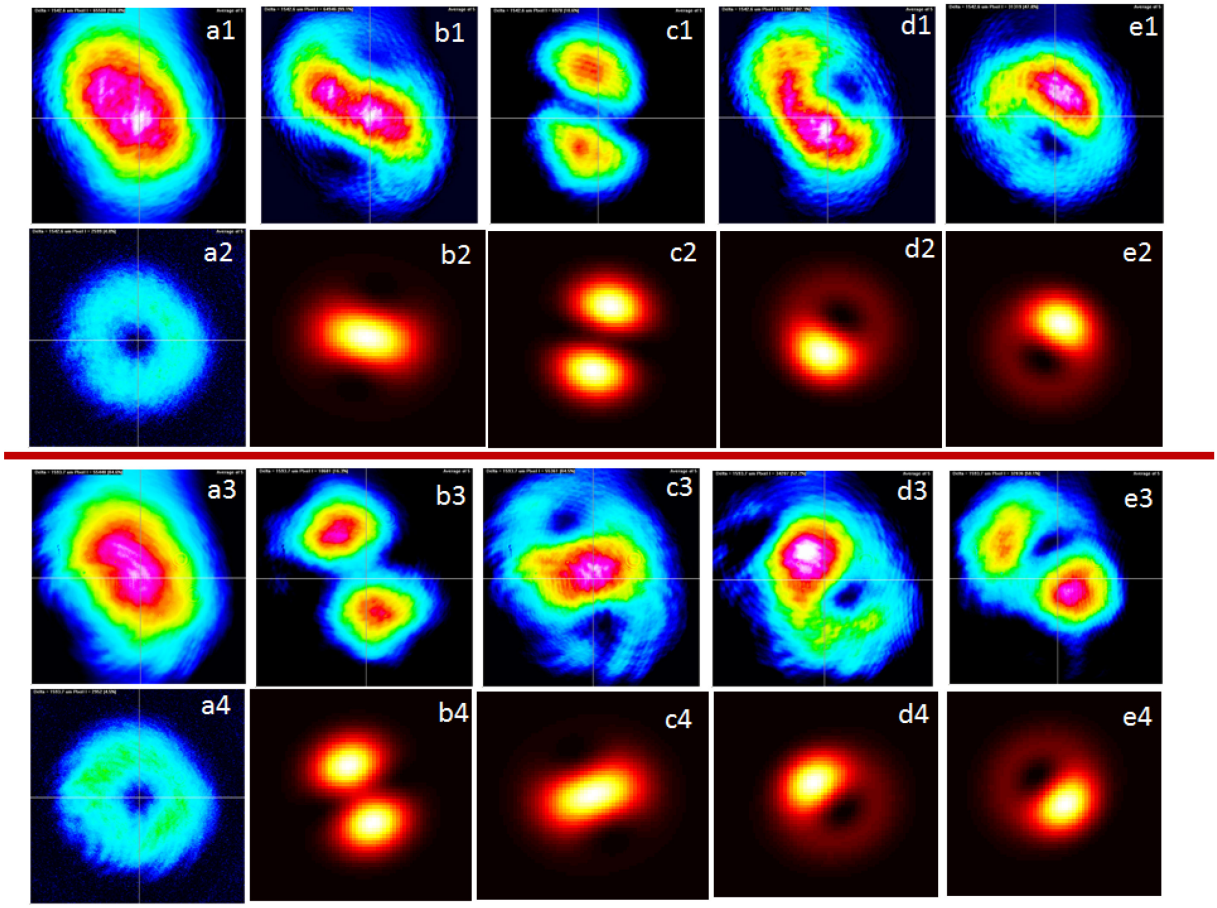

Fig. 3 Far field patterns recorded at 1068 nm except a2 and a4 pictures: 1064 nm. The upper and lower parts correspond to two slightly different crystal orientations (see text). Columns b, c, d and e correspond respectively to horizontal, vertical, circularly left and right polarizations. The full scale of all the pictures is ±11 mrad.

Lasing was studied under various crystal orientations, all such that they include a close alignment of the crystal optical axis and the cavity axis. The key-point is that the lasing direction is not unique, it does not reduce to the cavity direction, it is always constituted by an angular distribution given by the far field pattern (see for example a1 and a3 pictures in Fig. 3 in two crystal orientations detailed below) which can be compared with the optical axis direction (dark area centre in a2 and a4 pictures in Fig. 3). To operate this point, once all the far and near field wanted patterns have been recorded with the two cameras at 1068 nm, the M1 mirror was removed and a 1064 right circularly polarized laser beam (from an auxiliary laser) was injected along the cavity axis and analysed with a left circularly polarizer on the far field path. The well-known partial conoscopy pattern is constituted by a brilliant ring with a dark area inside, the optical axis direction being in the centre determined without ambiguity. We found that for each crystal orientation the 1068 nm laser far field included the 1064 nm central dark area (optical axis).

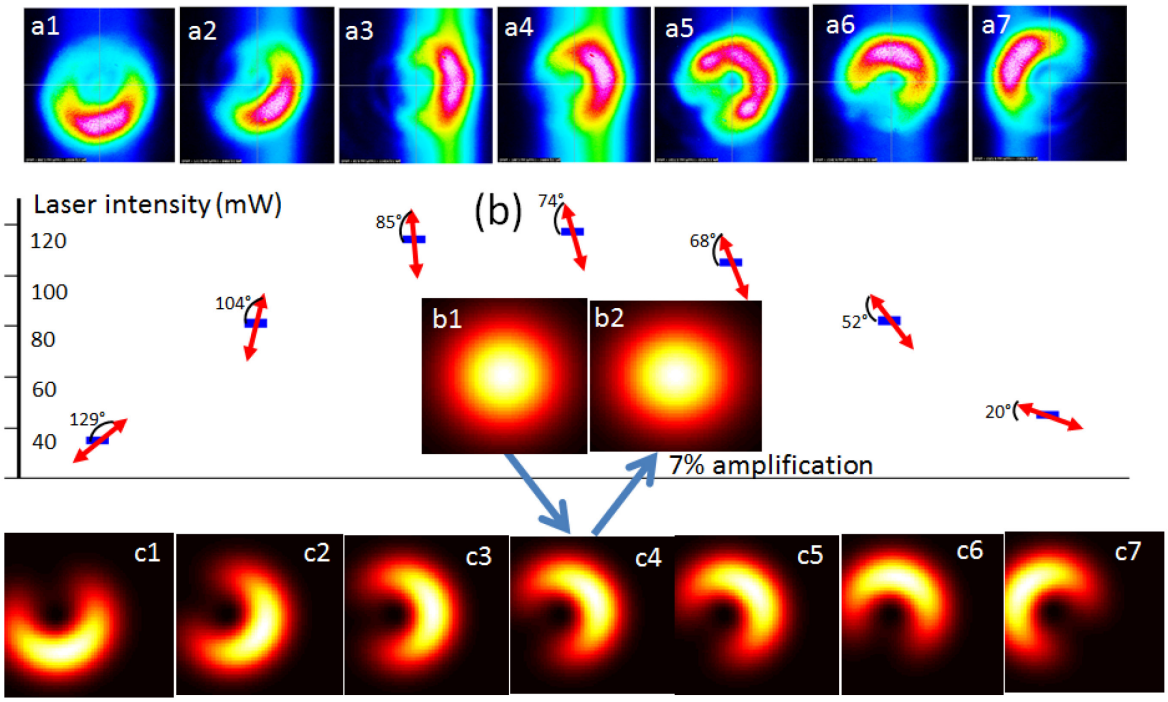

Fig. 4: a1-a7: experimental near field pattern on the M2 output mirror; (b) intensity and polarization of the laser escaping from the M1 mirror; b1: laser intensity at the entrance face of the crystal, b2: same as b1 after a cavity round trip; c1-c7: theoretical near field pattern on the M2 output mirror. The full scales of all the squares pictures are ±130 µm X ±130 µm.

The various crystal orientations of lasing were chosen trying to get, in practice as much as possible, a circular near field pattern on the M2 output mirror (projected and visualized on the CCD1 camera). Except in a very particular case exhibited below, we found in our self-conical diffraction experiment that it was not possible to get a full circle as in conical diffraction experiments using a controlled external laser beam. On the contrary attempts led to crescent shape light distributions around a circle (see the seven a1-a7 upper pictures in Fig. 4). The reason is that the laser beam reflected by the M1 mirror towards the laser crystal is strongly linearly polarized. This can be checked by testing the beam escaping from the M1 mirror with a linear polarizer. More precisely, with the help of an additional quarter-wave plate with its fast axis aligned with the minimum intensity direction transmitted by the polarizer, we can determined that the beam is composed by 95-90% linear polarized and 5-10% unpolarised. These directions of polarizations (M1 side) are represented by the red arrows in the central b picture in Fig 4, superimposed with the laser output power obtained under 0.77 W pumping (blue horizontal squares). These laser features (polarization and intensity) are in clear agreement with the fluorescence spatial distribution of the highest modes intensities as it was experimentally measured in ref. [4] in the vicinity of the optical axis: the polarization with the highest intensity is not far to vertical and the lowest intensity not far to horizontal.
The crystal orientations corresponding to a2 and a5 pictures in Fig. 4 have their far field patterns in various linear and circular polarizations represented in Fig 3 upper and lower parts respectively.
The theoretical model presented in section 2 was used with input Gaussian beams trough the M1 mirror having polarizations α =129°, 104°, 85°, 74°, 68°, 52° and 20° (Fig. 4 b) in comparison to x'-axis, so the input electric field in Eq. (13) was:

$$\begin{bmatrix}\hat{E}_{x'}(k_{ix'},k_{iy'})\\ \hat{E}_{y'}(k_{ix'},k_{iy'})\end{bmatrix}=\begin{bmatrix}\cos(\alpha)\\ \sin(\alpha)\end{bmatrix}\frac{2\pi b}{k_i}exp(-\frac{b}{2k_i}(k_{ix'}^2+k_{iy'}^2))\ \exp(ik_{iz'}z_C') \qquad (19)$$

where the central exponential originates from the Fourier transform of the Gaussian beam circulating between the M1 mirror and the KGW:Nd crystal, $z_C' = -1.7$ cm is the crystal entrance face position, $b = \frac{\pi w_0^2}{\lambda}$ is the confocal parameter. After discretisation the inverse Fourier transform in Eq. (16) was calculated with the inverse Fast Fourier Transform (iFFT) algorithm of the Mathlab package.

The calculated near field patterns (pictures c1-c7 in Fig. 4) are in reasonable agreement with the experimental data (pictures a1-a7 in Fig. 4). Despite of the fact that a full circle is not obtained due to the strongly linear polarization of the bean passing through the crystal, it is clear that the doughnut-like distribution that we can guess here is due to the value close to 1 of the ratio of the conical refraction ring radius and the laser waist, and this distribution structure would disappear increasing the laser waist by shortening the M1 arm. An agreement is also seen in Fig. 3: the far field patterns b2-e2 are similar to b1-e1 and the b4-e4 are similar to b3-e3.

We have also calculated the electric field of the wave reflected back by the M2 output plane mirror (where the wave-front is calculated to be plane) and going backwards through the laser crystal a second time. The example of the 74° polarization of the beam on the M1 side is detailed in Fig. 4 (b). Picture b1 represents the beam intensity at the entrance of the laser crystal, picture c4 is the beam on the output M2 mirror and picture b2 is the reflected beam intensity after a second pass through the laser crystal. We can see that after this round trip the Gaussian beam is reconstituted and more, its integrated intensity is 1.07 time the initial one. This amplification, calculated with 0.2079% fraction population inversion, is of course what is needed to compensate the transmissions of the two mirrors: 2% (M1) and 5% (M2). The fraction population inversion needed to have 7% round trip amplification for the 7 input polarization angles of Fig. 4 (b) is 0.2885%, 0.224%, 0.2059%, 0.2079%, 0.2125%, 0.238% and 0.348% respectively. Because it results of the same pumping rate in all cases, the lower the population inversion, the highest the laser intensity at steady state circulating inside the cavity. This is at least qualitatively in agreement with the laser intensity given in Fig. 4 (b). Let us add that the corresponding amplification coefficients (cm^{-1}) are directly obtained as the imaginary part of expressions (9-10) (see also ref. [4]) after averaging over the propagation directions.

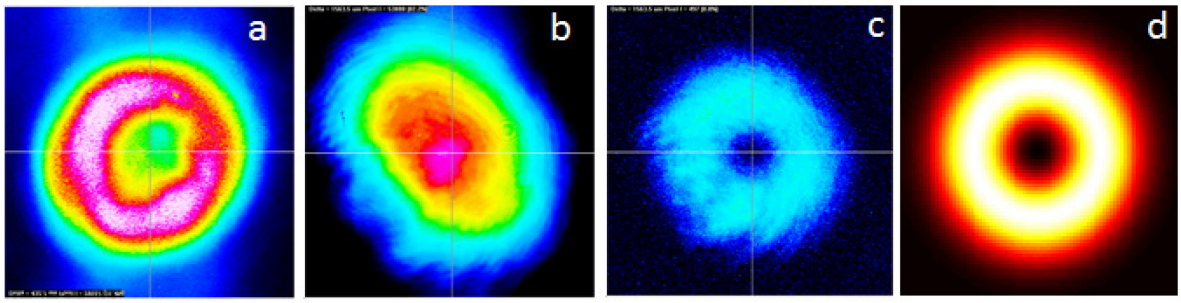

Fig. 5: (a) experimental and (d) theoretical near field patterns (see text), full scales ±130 X ±130 μm^2; (b) and (c): far field patterns at 1068 and 1064 nm respectively, full scales: ±11 mrad.

Finally, efforts to get a full circular near field pattern on the CCD1 camera led to the one represented in Fig. 5 (a). Its instability prevented a precise measurement of the power versus polarization on the M side, nevertheless it was clear that it was mainly un-polarized with 12-15 mW laser power. The laser far field pattern (Fig. 5 (b) shows that the lasing directions distribution contains the optical axis direction (centre of Fi. 5 (c)). The near field theoretical description was obtained by averaging the near field intensities corresponding to a continuous distribution of α angles launched towards the crystal from the M1 side. The result (Fig. 5 (d)) is in reasonable agreement with the experimental data (Fig. 5 (a)).

5. Conclusion

We have used an experimental set-up specially designed to determine simultaneously the far field and the near field patterns of lasing in the conditions for conical diffraction in the biaxial KGW:Nd crystal. The key-point is that the lasing direction is not unique and does not reduce to the cavity direction, it is always constituted by an angular distribution including the optical axis. We checked this with the help of the far field patterns at 1064 and 1068 nm. Very slight changes of crystal orientation leads to crescent shape 1068 nm light distributions in the near field (output mirror) around the well-known ring characterizing the internal conical refraction. This can be explained because the beam launched towards the biaxial crystal is mainly linear polarized with its intensity closely in agreement with the Nd fluorescence spatial distribution determined in a separate work. In a very particular crystal position, a beam mainly un-polarized was obtained with a near field distribution almost circular. A theoretical background is provided, including the case of monoclinic and triclinic symmetries and laser amplification including elliptical modes and cavity round trip. The calculation is in reasonable agreement with all the experimental data (near and far fields).

References

1. Voigt W, "On the behaviour of pleochroitic crystals along directions in the neighbourhood of an optic axis", Phil. Mag. S. 6, **4**, 90-97 (1902).
2. S. Pancharatnam, "On the pleochroism of amethyst quartz and its absorption spectra", Proc. Ind. Acad. Sci. A, **40 A**, 196-210 (1954).
3. S. Pancharatnam, "The propagation of light in absorbing biaxial crystals", Proc. Ind. Acad. Sci. **42 A**, 86-109 and 235-248 (1955).
4. A. Brenier, "Polarization properties of lasing near an optical axis in the biaxial $KGd(WO_4)_2$:Nd crystal", Las. Phys. Lett. **11**, 115819-115826 (2014).
5. A. Brenier, "Voigt wave investigation in the $KGd(WO_4)_2$:Nd biaxial laser crystal", J. Opt. 17, 075603 (2015).
6. J. Gerardin, A. Lakhtakia, "Conditions for Voigt wave propagation in linear, homogenous, dielectric medium"s, Optik **112**, 493-495 (2001).
7. Tom G. Mackay, J. Nanophot. "On the sensitivity of directions that support Voigt wave propagation in infiltrated biaxial dielectric materials", 8, 083993 (2014).
8. M. Born, E. Wolf, A. B. Bhatia, *Principles of optics: electromagnetic theory of propagation, interference and diffraction of light*, 7th ed. Cambridge University Press, 1999.
9. L. Landau and E. Lifchitz, *Electrodynamique des milieux continus, Ed. Mir Moscou* 1969.
10. A. M. Belskii and A. P. Khapalyuk, "Propagation of confined light beams along the beam axes of biaxial crystals", Opt. Spectrosc. (USSR) 44 (3) 312-315 (1978)
11. A. M. Belskii and A. P. Khapalyuk, "Internal conical refraction of bounded light beams in biaxial crystals", Opt. Spectrosc. (USSR) 44 (4) 436-438 (1978)

12. A. M. Belskii and M. A. Stepanov, “Internal conical refraction of coherent light beams”, Opt. Comm. 167, 1-5 (1999).
13. M. V. Berry, “Conical diffraction asymptotics: fine structure of Poggendorff rings and axial spikes”, J. Opt. A: Pure Appl. Opt. 6, 289-300 (2004).
14. M. V. Berry, M. R. Jeffrey and J. G. Lunney, “Conical diffraction: observation and theory”, Proc. R. Soc. A, **462**, 1629-1642 (2006).
15. A. Turpin, Y. Loiko, T. Kalkandjiev, J. Mompart, “Free-space optical polarization demultiplexing and multiplexing by means of conical refraction”, Opt. Lett. **37**, 4197-4199 (2012).
16. D. P. O’Dwyer, K. E. Ballantine, C. F. Phelan, J. G. Lunney, J. F. Donegan, “Optical trapping using cascade conical refraction of light”, Opt. Exp. **20**, 21119-21121 (2012).
17. S. Rosen, G. Y. Sirat, H. Ilan, and A. J. Agranat, “A sub wavelength localisation scheme in optical imaging using conical refraction”, Opt. Exp. 21, 10133-10138 (2013).
18. Julien Caron, Clément Fallet, Jean-Yves Tinevez, Lionel Moisan, L Philippe (Ori) Braitbart, Gabriel Y. Sirat, and Spencer L Shorte, “Conical diffraction illumination opens the way for low phototoxicity super-resolution imaging”, Cell Adhesion & Migration, 8:5, 430-439 (2015).
19. C. F. Phelan, R. J. Winfield, D. P. O’Dwyer, Y. P. Rakovich, J. F. Donegan, and J. G. Lunney, Opt. Commun. 284, 3571-3574 (2011).
20. Alba Peinado, Alex Turpin, Angel Lizana, Estefania Fernández, Jordi Mompart, and Juan Campos, "Conical refraction as a tool for polarization metrology," Opt. Lett. 38, 4100-4103 (2013).
21. Stephen D Grant, Steve Reynolds and Amin Abdolvand, “Optical sensing of polarization using conical diffraction phenomenon,” J. Opt. 18, 025609 (2016).
22. V. Peet, “Biaxial crystals as a versatile mode converter”, J. Opt. 12, 5706 (2010).
23. V. Peet, “Improving directivity of laser beams by employing the effect of conical refraction in biaxial crystals”, Opt. Exp. 18, 19566-19573 (2010).
24. G. S. Sokolovskii, D. J. Carnegie, T. K. Kalkandjiev, E. U. Rafailov, “Conical refraction: New observations and a dual cone model”, Opt. Exp. 21, 11125-11131 (2013).
25. A. Turpin, Yu. V. Loiko, T. K. Kalkandjiev, H. Tomizawa, J. Mompart, “Super-Gaussian conical refraction beams”, Opt. Lett. 39, 4349-4352 (2014).
26. S. D. Grant and A. Abdovland, “Evolution of conically diffracted Gaussian beams in free space”, Opt. Exp. 22, 3880-2886 (2014).
27. A. Turpin, Yu. V. Loiko, A. Peinado, A. Lizana, T. K. Kalkandjiev, J. Campos, J. Mompart, “Polarization tailored novel vector beams based on conical refraction”, Opt. Exp. 23, 5704-5715 (2015).
28. A. Turpin, Yu. V. Loiko, T. K. Kalkandjiev, J. Mompart, “Light propagation in biaxial crystals”, J. Opt. 17, 065603 (2015).
29. A. Turpin, Yu. V. Loiko, T. K. Kalkandjiev, H. Tomizawa, J. Mompart, “On the dual cone nature of the conical refraction phenomenon”, Opt. Lett. 40, 1639-1642 (2015).
30. J. Hellstrom, H. Henricsson, V. Pasiskevicius, U. Bunting, D. Haussmann, “Polarization-tunable Yb:KGW laser based on internal conical refraction”, Opt. Lett. **32**, 2783-2785 (2007).
31. K. G. Wilcox, A. Abdolvand, T. K. Kalkandjiev, E. U. Rafailov, “Laser with simultaneous Gaussian and conical refraction outputs”, Appl. Phys. B Lasers and Optics 99, 619-622 (2010).

32. A. Abdolvand, K. G. Wilcox, T. K. Kalkandjiev, E. U. Rafailov, “Conical refraction Nd:$KGd(WO_4)_2$ laser”, Opt. Exp. 18, 2753-2759 (2010).
33. Y. V. Loiko, G. S. Sokolovskii, D. Carnegie, A. Turpin, J. Mompart, E. Rafailov, “Laser beams with conical refraction patterns”, Proc. SPIE 8960, 89601Q (2014).
34. Romain Cattoor, Inka Manek-Hönninger, Daniel Rytz, Lionel Canioni, and Marc Eichhorn, "Laser action along and near the optic axis of a holmium-doped KY(WO4)2 crystal," Opt. Lett. 39, 6407-6410 (2014).
35. I. V. Mochalov, “Laser and nonlinear properties of the potassium gadolinium tungstate laser crystal $KGd(WO_4)_2:Nd^{3+}$ (KGW:Nd)”, Opt. Eng. **36**, 1660-1669 (1997).
36. N. S. Ustimenko and A. V. Gulin, “New self-frequency converted Nd^{3+}:$KGd(WO_4)_2$ Raman lasers”, Quant. Electr. **32**, 229-231 (2002).
37. Y. Chen, Y. Lin, X. Gong, Q. Tan, J. Zhuang, Z. Luo, Y. Huang, “Polarized spectroscopic properties of Nd^{3+}-doped $KGd(WO_4)_2$ single crystal”, J. Lumin. **126**, 653-660 (2007).
38. Y. Petit , B. Boulanger , P. Segond, C. Félix, B. Ménaert , J. Zaccaro , G. Aka, “Absorption and fluorescence anisotropies of monoclinic crystals : the case of Nd :YCOB”, Opt. Exp. **16** (11) 7997-8002 (2008).
39. A. Brenier, Y. Wu, J. Zhang, Y. Wu, P. Fu, “Lasing Yb^{3+} in crystals with a wavelength dependence anisotropy displayed from $La_2CaB_{10}O_{19}$”, Appl. Phys. B: Lasers and Optics **107**, 59-65 (2012).
40. R. M. Solé, M. C. Pujol, J. Massons, M. Aguiló, F. Díaz and A. Brenier, “Growth, anisotropic spectroscopy and lasing of the monoclinic Nd:$KGd(PO_3)_4$ crystal”, J. Phys. D: Appl. Phys. **48**, 495502-49512 (2015).

Figure captions

Fig. 1 (a) Crystal orientation and useful frameworks, (b) Refraction law illustrated in the incidence plane (=Figure plane; the Ox'y' face is perpendicular to the incidence plane).

Fig. 2 Lasing set-up and optical paths for far field and near field analysis.

Fig. 3 Far field patterns recorded at 1068 nm except a2 and a4 pictures: 1064 nm. The upper and lower parts correspond to two slightly different crystal orientations (see text). Columns b, c, d and e correspond respectively to horizontal, vertical, circularly left and right polarizations. The full scale of all the pictures is ±11 mrad.

Fig. 4: a1-a7: experimental near field pattern on the M2 output mirror; (b) intensity and polarization of the laser escaping from the M1 mirror; b1: laser intensity at the entrance face of the crystal, b2: same as b1 after a cavity round trip; c1-c7: theoretical near field pattern on the M2 output mirror. The full scales of all the squares pictures are ±130 µm X ±130 µm.

Fig. 5: (a) experimental and (d) theoretical near field patterns (see text), full scales ±130 X ±130 μm^2; (b) and (c): far field patterns at 1068 and 1064 nm respectively, full scales: ±11 mrad.